

SOLITONS AND OPTICAL FIBRES

PACS numbers: 42.81.Dp; 42.65.Tg
DOI: 10.1070/QE2002v032n11ABEH002338

Multiwavelength pulse transmission in an optical fibre – amplifier system

N.-C. Panoiu, I.V. Mel'nikov, D. Mihalache, C. Etrich, F. Lederer

***Abstract*. The structure and dynamics of solitary waves created in the interaction of multiwavelength pulses in a single-mode optical fibre with amplification, filtering, and amplitude modulation is analysed. It is shown that there is a critical wavelength separation between channels above which wavelength-division multiplexing with solitons is feasible and that this separation increases with the number of channels.**

Keywords: *soliton, fibre amplifier, wavelength-division multiplexing*.

1. Introduction

In the last decade, considerable progress has been achieved in experiments on fibreoptic long-distance soliton data transmission with wavelength-division multiplexing (WDM) [1, 2]. When compared to conventional single-channel soliton systems, WDM offers the potential for a considerable increase in the total capacity of soliton-based communication devices. However, the use of WDM raises a number of issues of both fundamental and practical importance. First, the intrinsic Kerr nonlinearity of silica that is used to balance the dispersion also causes interaction among neighboring solitons. This interaction exists even if all external perturbative factors are removed, i.e., in physical situations when solitons are supposed to propagate freely, and limits the bit rate of a soliton-based transmission system [3 – 6]. Moreover, due to the periodic distribution of amplifiers, a resonant instability created by nonlinear terms can seriously degrade the signal. In WDM soliton systems, there can also be serious timing displacement effects due to inelastic soliton collisons in the presence of amplifiers which induce permanent velocity and carrier frequency shift of the solitons [7 – 10]. Therefore, in order to be able to reduce such deterimental effects, it is important to understand the interaction of superimposed solitons which propagate at different wavelengths through a communication line in the presence of perturbations such as fibre amplifiers, filters, etc.

In this article, we present a comprehensive description of the structure of the optical field generated by the superposition of soliton-like optical pulses propagating in different channels. The article is organised as follows. In Section 2, we analyse the structure of the optical field resulting from the general superposition of two soliton-like optical pulses propagating in different channels. Then, in Section 3, by using the adiabatic perturbative approach, we describe the propagation of the emerging two-soliton solutions in the presence of external perturbations relevant for optical communication systems. The more general case of the superposition of N soliton-like pulses is discussed in Section 4. Finally, in the last section, the results are summarised and discussed.

2. Optical output from a two-soliton superposition

In this section we study the structure of the optical field emerging from a superposition of two soliton-like optical pulses with different frequencies. We begin by considering first two particular cases, namely, the two input pulses are in-phase or out-of-phase, and then we discuss the general case in which the phase shift between the two pulses is arbitrary.

In the case of the negative dispersion and Kerr nonlinearity of the fibre, the pulse evolution obeys the following nonlinear Schrödinger equation (NLSE):

$$i\psi_z + \psi_{tt} + 2|\psi|^2\psi = 0, \tag{1}$$

where ψ is the normalised complex amplitude of the pulse; $z = |\beta_2|Z/2\tau^2$ is the normalised propagation distance; $t = (T - Z/v_g)/\tau$ represents the normalised time; β_2 is the group-velocity dispersion; τ is the pulse width; v_g is the group velocity, and Z and T are the physical distance and time, respectively.

2.1 In-phase pulses

To begin with, let us consider the following symmetric (in-phase) superposition of solitons,

$$\psi(0, t) = \mathrm{sech}t \exp(i\omega t/2) + \mathrm{sech}t \exp(-i\omega t/2), \tag{2}$$

N.-C. Panoiu Department of Applied Physics and Applied Mathematics, Columbia University, New York, New York 10027;
I.V. Mel'nikov [Permanent address] A.M. Prokhorov General Physics Institute, Russian Academy of Sciences, ul. Vavilova 38, Moscow 119991, Russia; Department of Electrical and Computer Engineering, University of Toronto, 10 King's College Road, Toronto, Ontario M5S 1A4, Canada;
D. Mihalache [Permanent address] Department of Theoretical Physics, Institute of Atomic Physics, PO BOX MG-6, Bucharest, Romania;
C. Etrich, F. Lederer Institute of Solid State Theory and Theoretical Optics, Friedrich Schiller University Jena, Max-Wien-Platz 1, Jena, D-07743, Germany

Received 17 June 2002
Kvantovaya Elektronika **32** (11) 1009 – 1016 (2002)
Submitted in English

where ω is the frequency separation between the two channels. If the initial condition $\psi(0,t)$ is a symmetric function $[\psi(t)=\psi(-t)]$, the associated scattering coefficient $a(\lambda)$ of the inverse scattering problem, whose zeros determines the soliton parameters, has the symmetry property $a(\lambda)=a^*(-\lambda^*)$, where the asterisk means complex conjugation. Therefore, the zeros of $a(\lambda)$ are located on the imaginary axis or appear in pairs at $(\lambda,-\lambda^*)$. Since it will play an important role in our further discussion, we give here the solution which corresponds to a pair $(\lambda_0,-\lambda_0^*)$ of zeros situated symmetrically with respect to the imaginary axis [11]

$$\psi(z,t)=-\mathrm{i}\zeta\eta\mathrm{e}^{[\phi(z)+\alpha]}\times$$

$$\frac{\mathrm{e}^{\mathrm{i}\zeta t}\cosh[\eta t+\rho(z)+\mathrm{i}\varphi]+\mathrm{e}^{-\mathrm{i}\zeta t}\cosh[\eta t-\rho(z)-\mathrm{i}\varphi]}{\zeta^2\cosh[\eta t-\rho(z)]\cosh[\eta t-\rho(z)]+\eta^2\sin[\zeta t+\mathrm{i}\rho(z)]\sin[\zeta t-\mathrm{i}\rho(z)]}. \tag{3}$$

Here, $\lambda_0=\xi+i\eta$, $\phi(z)=-i(\xi^2+\eta^2)z+\phi_0$, $\rho(z)=2\xi\eta z+\rho_0$, $\alpha=\ln|\lambda_0|$, and $\varphi=\eta/\zeta;\eta,\zeta$. As can be easily seen, the symmetry of the solution is preserved during the propagation: $\psi(z,t)=\psi(z,-t)$.

In order to describe the structure of the optical field emerging from the superposition (2), we determined the spectrum of the linear eigenvalue problem, which corresponds to the input (2) (i. e., the zeros of $a(\lambda)$ located on the imaginary axis as well as the function $a(\lambda)$ for $\lambda\in\{\Re\}$). The numerical method used is based on an algorithm introduced in Ref. [12].

The main results are illustrated by the Fig. 1a, where the soliton spectrum is presented. One can see that three different kinds of solitons can be generated. First, for $\omega<\omega_1^{\mathrm{s}}\simeq 1.01$, the coefficient $a(\lambda)$ has two distinct zeros located on the imaginary axis, so that a bound state consisting of two solitons with zero velocities (breather) emerges. At $\omega_1^{\mathrm{s}}<\omega<\omega_2^{\mathrm{s}}\simeq 2.626$, the coefficient $a(\lambda)$ has only one zero located on the imaginary axis, so that only a single soliton with zero velocity can be generated. If the frequency ω is further increased, $\omega_2^{\mathrm{s}}<\omega<\omega_3^{\mathrm{s}}\simeq 3.018$, again the coefficient $a(\lambda)$ has two zeros on the imaginary axis, so that again a breather emerges. If $\omega_3^{\mathrm{s}}<\omega$, the coefficient $a(\lambda)$ has two zeros situated symmetrically with respect to the imaginary axis, so that the emerging solution is the two-soliton solution (3).

By using the expression for the input pulse and the scattering data, we calculate next the total energy E_{in} of the initial pulse, the energy E_{sol} of the emerging solitons and the energy E_{rad} in the radiative modes. They are defined as

$$E_{\mathrm{in}}=\int_{-\infty}^{\infty}|\psi(x,0)|^2\mathrm{d}x, \tag{4}$$

$$E_{\mathrm{sol}}=2\sum_{i=1}^{n}\eta_i, \tag{5}$$

$$E_{\mathrm{rad}}=-\frac{1}{\pi}\int_{-\infty}^{\infty}\ln|a(\lambda)|\mathrm{d}\lambda, \tag{6}$$

and do not change upon propagation. Moreover, they must satisfy the relation $E_{\mathrm{in}}=E_{\mathrm{sol}}+E_{\mathrm{rad}}$.

The dependence of E_{in} and E_{rad} on ω is presented in Fig. 1b. An important fact this figure illustrates is that the energy of the radiative modes has two peaks at the threshold frequencies ω_1^{s} and ω_2^{s}. Consequently, the generated solitons are influenced by the radiative field, especially when the frequency detuning ω is close to these two threshold values. The origin of these two peaks can be understood if we take into account the spectrum shown in Fig. 1a. Thus, for $\omega=\omega_{1,2}^{\mathrm{s}}$, the scattering coefficient $a(\lambda)$ has a zero in origin. Therefore, the integrand in Eqn (6) has a logarithmic singularity at these two critical values of the frequency detuning ω.

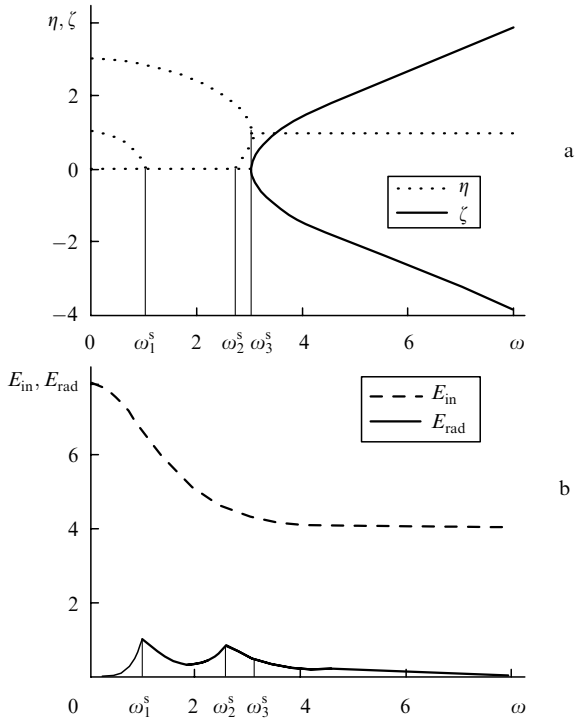

Figure 1. The discrete spectrum determined by the symmetric input (*2*) and the energies in the optical field at the output. (a) The amplitude η (dotted curve) and the velocity ξ (solid curve) of the generated solitons as a function of ω; (b) The energies E_{in} (dashed curve) and E_{rad} (solid curve) vs ω.

2.2 Out-of-phase pulses

The second case we analyse is the generation of solitons from an antisymmetric superposition of two soliton-like pulses. The input pulse is described by the expression:

$$\psi(0,t)=\mathrm{i}[\mathrm{sech}t\exp(\mathrm{i}\omega t/2)-\mathrm{sech}t\exp(-\mathrm{i}\omega t/2)]. \tag{7}$$

Here, the imaginary unit was introduced only to ensure that the initial condition $\psi(0,t)$ is a real function. As before, the symmetry property $\psi(t)=-\psi(-t)$ implies that the zeros of the scattering coefficient $a(\lambda)$ are purely imaginary or are located symmetrically with respect to the imaginary axis. In this case, the two-soliton solution, which corresponds to such a pair of zeros, is given by the expression:

$$\psi(z,t)=-\mathrm{i}\zeta\eta\mathrm{e}^{[\phi(z)+\alpha]}\times$$

$$\frac{\mathrm{e}^{\mathrm{i}\zeta t}\cosh[\eta t+\rho(z)+\mathrm{i}\varphi]-\mathrm{e}^{-\mathrm{i}\zeta t}\cosh[\eta t-\rho(z)-\mathrm{i}\varphi]}{\zeta^2\cosh[\eta t+\rho(z)]\cosh[\eta t-\rho(z)]+\eta^2\cos[\zeta t+\mathrm{i}\rho(z)]\cos[\zeta t-\mathrm{i}\rho(z)]}. \tag{8}$$

As before, we calculate the soliton spectrum, which corresponds to the choice (7). The structure of this spectrum, as well as the dependence of the energies $E_{\rm in}$ and $E_{\rm rad}$ on the frequency detuning ω, is shown in Fig. 2. As Fig. 2a illustrates, for frequency detuning $\omega < \omega_1^{\rm s} \simeq 0.738$, no soliton is generated, while for $\omega > \omega_1^{\rm s}$ the emerging field is the two-soliton solution described by Eqn (8). Unlike the symmetric case, for antisymmetric input pulses with $\omega \simeq \omega_1^{\rm s}$, the emerging soliton is observed to have a finite velocity. This fact can be understood as follows: if both the velocity ξ and the amplitude η would vanish, then the coefficient $a(\lambda)$ would have a zero in origin. It is shown, however, in the next subsection, that this would require the area of the input pulse to be an odd multiple of $\pi/2$, a condition which cannot be satisfied by an antisymmetric function. Finally, similar to the symmetric case, the energy in the radiative modes $E_{\rm rad}$ has a maximum at $\omega = \omega_1^{\rm s}$.

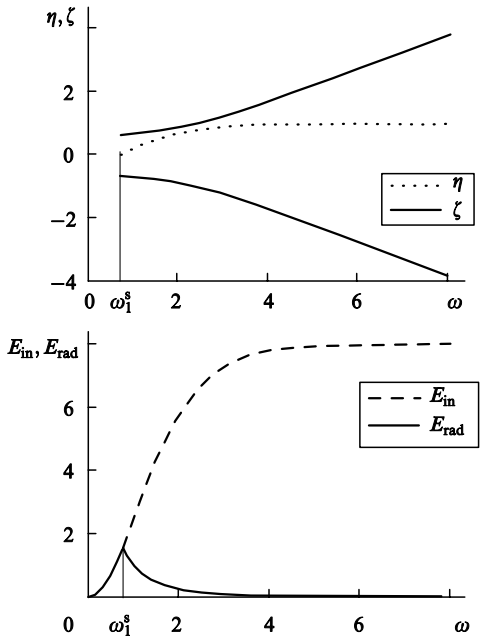

Figure 2. The same as in Fig. 1 but for the antisymmetric input (7).

2.3 Arbitrary phase shift

In this subsection, we discuss the general situation, in which there is an arbitrary phase shift between the two overlapping solitons. This kind of input is described by the expression

$$\psi(0,t) = \mathrm{sech}t \exp[\mathrm{i}(\omega t + \theta)/2] + \mathrm{sech}t \exp[-\mathrm{i}(\omega t + \theta)/2], \quad (9)$$

where θ is the phase difference between the two solitons. In order to understand the structure of the emerging optical field, which corresponds to an arbitrary value of the phase shift θ, we use the relation [13]

$$a(0) = \cos S_0, \quad (10)$$

where S_0 is the initial area of the pulse. Note that Eqn (10) holds only for pulses which are real up to a constant overall phase. Now let us see how Eqn (10) can be used to explain the structure of the soliton spectrum and, consequently, the structure of the emerging optical field. The initial area of the optical pulse described by Eqn (9) is

$$S_0(\omega,\theta) = 2\pi\mathrm{sech}(\pi\omega/4)\cos(\theta/2). \quad (11)$$

One can see from Eqns (10) and (11) that if $\omega = 0$, there are two critical values of the phase difference θ for which $a(0) = 0$. The two critical values are $\theta_{\rm cr}^{(1)} = 2\arccos(3/4)$ and $\theta_{\rm cr}^{(2)} = 2\arccos(1/4)$ and correspond to $n = 2$ and $n = 1$, respectively. This implies that at $\omega = 0$, depending on the value of the phase difference θ, there are two distinct zeros of $a(\lambda)$ located on the imaginary axis, if $0 \leqslant \theta < \theta_{\rm cr}^{(1)}$, one, if $\theta_{\rm cr}^{(1)} < \theta < \theta_{\rm cr}^{(2)}$, and none, if $\theta_{\rm cr}^{(2)} < \theta \leqslant \pi$. Consequently, the soliton spectra in the first and the third case are topologically similar to the ones presented in Fig. 1a and Fig. 2a, respectively. A typical spectrum which corresponds to the second case, i.e., $\theta_{\rm cr}^{(1)} < \theta < \theta_{\rm cr}^{(2)}$, is presented in Fig. 3. We emphasise that in order to generate solitons of the type (3) and (8), the choice of the initial pulses is not restricted to sech-like type. Thus, we calculated the structure of the emerging solitons from a superposition of two Gaussian pulses, and the results obtained were qualitatively similar to those presented here. As a final remark, we mention that in a WDM transmission line, the relative phase between the initial pulses in different channels is not the same for all the pairs in the pulse train. However, the results presented here can serve as a first step towards a general description of a more realistic situation in which the relative phase between adjacent pulses varies randomly.

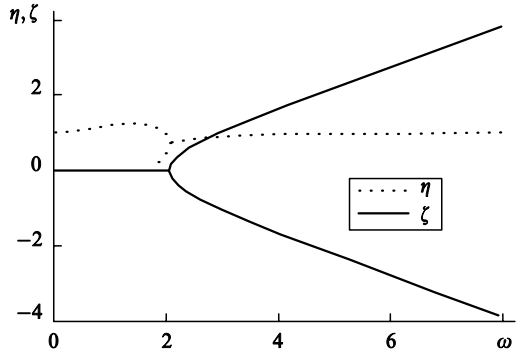

Figure 3. The discrete spectrum determined by Eqn (9). The amplitude η (dotted curve) and the velocity ξ (solid curve) of the generated solitons vs ω. The phase difference is $\theta = 2\pi/3$.

3. Perturbative propagation of two-soliton solutions

As shown above, solitons described by Eqns (3) and (8) can be obtained from a superposition of optical pulses of a rather general shape. In practice, however, one is interested not only in the conditions under which one can generate such pulses but also in how they propagate along an optical transmission line in the presence of perturbations, when soliton parameters such as amplitude and velocity become dependent on the propagation distance.

In order to determine the shape of the propagating optical pulse in the presence of weak perturbations, we

resort to both adiabatic perturbation theory and direct numerical integration of the NLSE (1) perturbed by a term $\varepsilon P(\psi,\psi^*)$,

$$i\psi_z + \psi_{tt} + 2|\psi|^2\psi = \varepsilon P(\psi,\psi^*). \quad (12)$$

If $\varepsilon \ll 1$, the evolution of the soliton parameters with respect to the propagation distance is given by a set of differential equations, which are fully determined by the perturbation $P(\psi,\psi^*)$ (for details, see Ref. [11]),

$$\frac{dS\{\psi,\psi^*\}}{dz} = \int_{-\infty}^{\infty} dt F\{P(\psi,\psi^*)P^*(\psi,\psi^*); S(\psi,\psi^*)\}, \quad (13)$$

where S is the set of scattering data and F is a functional, which depends both on the scattering data S and the perturbation P. Thus, if one knows the initial values of the soliton parameters one can integrate Eqn (13) and then, from the values obtained for the soliton parameters, can reconstruct the soliton solution at that propagation distance. Alternatively, one can integrate directly Eqn (12) with the specified initial conditions. In what follows, we will use both these methods to describe the propagation of the two-soliton solutions (3) and (8) in the presence of various perturbations.

3.1 Soliton propagation in the presence of lumped amplifiers, band-pass filters, and nonlinear amplifiers

Due to the inherent losses in a long-haul transmission line, optical pulses can propagate over long distances only if amplifiers are inserted periodically. Usually, the distance between the amplifiers is $z_a \simeq 50 - 80$ km. However, due to the excess gain introduced by the amplifiers, the dispersive wave noise increases exponentially with the propagation distance, leading to the instability of the soliton propagation. In order to overcome this problem, a nonlinear amplifier can be used [14, 15], and the averaged equation describing optical pulse propagation in a transmission line with such nonlinear amplifiers inserted periodically can be rewritten as:

$$i\psi_z + \psi_{tt} + 2|\psi|^2\psi = i\delta\psi + i\beta\psi_{tt} + i\gamma|\psi|^2\psi. \quad (14)$$

Here, $\gamma = 2g_0/z_a$, where the parameter g_0 characterises the averaged nonlinear gain over the amplifier span

$$g(|\psi|^2) = z_a^{-1}\ln\left(G|\psi|^2\right), \quad (15)$$

with $G = 1 + g_0|\psi|^2$ being the gain characteristic function of the nonlinear amplifier.

Obviously, Eqn (14) can be written in the form (12), with $\varepsilon = i\delta$ and the perturbation $P(\psi,\psi^*)$ given by:

$$P(\psi,\psi^*) = \psi + \varkappa_1\psi_{tt} + \varkappa_2|\psi|^2\psi. \quad (16)$$

The coefficients $\varkappa_1 = \beta/\delta$ and $\varkappa_2 = \gamma/\delta$.

The numerical simulations of Eqn (14) with the initial symmetric and antisymmetric two-soliton solutions show that when the condition $\varkappa_1 = 3 + 2\varkappa_2$ is satisfied, these solutions evolve into a pair of solitons with zero velocities and amplitudes equal to unity. Moreover, we observed that no significant amount of radiation is generated.

We also used the adiabatic perturbation method to investigate the evolution of the two-soliton solutions under the influence of the perturbation (16). The results are shown in Fig 4 for the symmetric and antisymmetric solitons, respectively. In each figure, three cases are presented and, as one can see, only in the case described by the coefficients $\varkappa_1 = 7$ and $\varkappa_2 = 2$, the soliton parameters approach asymptotically the values $(\xi_{as}, \eta_{as}) = (0, 1)$. This fact confirms that, as in the single soliton case, the propagation of a two-soliton solution is stabilised only if the relation $\varkappa_1 = 3 + 2\varkappa_2$ is satisfied. In the other two cases, i.e., if $\varkappa_1 < 3 + 2\varkappa_2$ ($\varkappa_1 > 3 + 2\varkappa_2$), the soliton amplitude increases (decreases). Furthermore, in all cases, the soliton velocity decreases to zero.

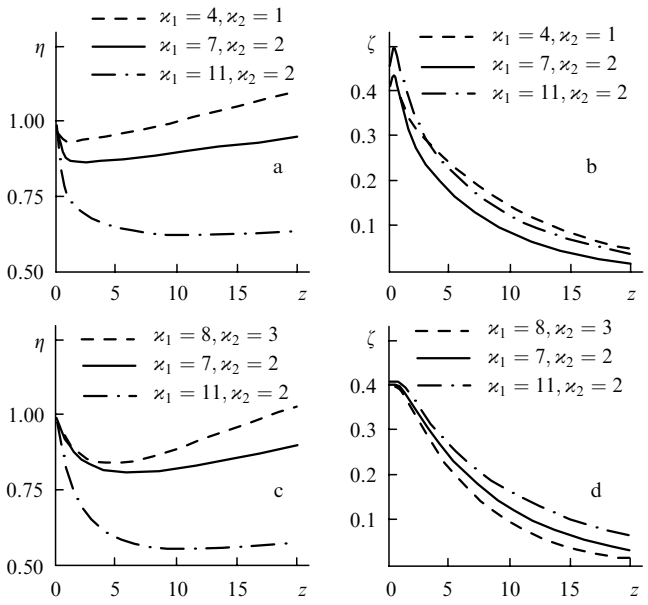

Figure 4. The soliton amplitude and velocity vs the propagation distance: $\delta = 0.02$ and the ratios $\varkappa_1 = 4$, $\varkappa_2 = 1$ in (a)–(b) and $\varkappa_1 = 8$, $\varkappa_2 = 3$ in (c)–(d) (dashed curve); $\varkappa_1 = 7$, $\varkappa_2 = 2$ (solid curve); $\varkappa_1 = 11$, $\varkappa_2 = 2$ (dotted-dashed curve). (a) The amplitude η of the symmetric soliton (3) with $\eta(0) = 1$, $\xi(0) = 0.4$, $\rho_0(0) = 0$, $\phi_0(0) = \pi/2$; (b) the velocity ξ of the symmetric soliton (3) with the same parameters as in (a); (c) the amplitude η of the antisymmetric soliton (8) with $\eta(0) = 1$, $\xi(0) = 0.4$, $\rho_0(0) = \phi_0(0) = 0$; (d) the velocity ξ of the antisymmetric soliton (8) with the same parameters as in (c).

In order to see how reliable are the results obtained by the perturbation method, we compared the optical fields obtained by the direct numerical simulations of Eqn (14) with those obtained by the perturbative method. The propagation distance was equal to 20 units in both cases. The results are presented in Fig 5 and correspond to the symmetric case. As these figures illustrate, there is a very good agreement between the two methods, so that one can conclude that the perturbation method describes properly the soliton interaction. Moreover, we mention that a very good agreement has been observed for the antisymmetric case as well.

3.2 Soliton propagation in the presence of lumped amplifiers, band-pass filters, and amplitude modulators

A different approach to overcome the limitations imposed by the bandwidth-limited amplification (BLA) on the efficiency of the soliton transmission system is to use an amplitude modulator (AM) inserted into the repeater loop

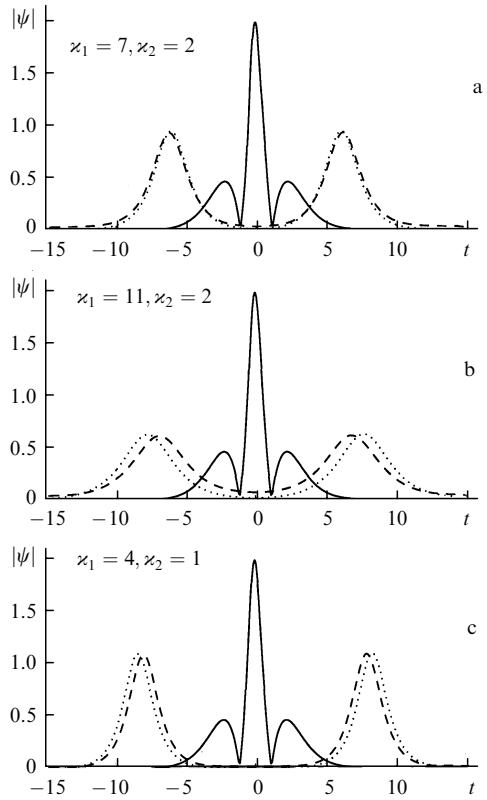

Figure 5. The amplitude $|\psi|$ of the symmetric soliton (3) with $\eta(0) = 1$, $\xi(0) = 0.4$, $\rho_0(0) = 0$, $\phi_0(0) = \pi/2$ after 20 propagation units: input pulse (solid curve), numerical simulations (dashed curve), adiabatic perturbation method (dotted line); $\delta = 0.02$. (a) $\varkappa_1 = 7$, $\varkappa_2 = 2$; (b) $\varkappa_1 = 11$, $\varkappa_2 = 2$; (c) $\varkappa_1 = 4$, $\varkappa_2 = 1$.

[16]. In this case, the soliton propagation is governed by the averaged equation:

$$i\psi_z + \psi_{tt} + 2|\psi|^2\psi = i\delta\psi + i\beta\psi_{tt} + i\mu_a[\cos(\Omega_a t) - 1]\psi, \quad (17)$$

where μ_a is the effective loss modulation; and Ω_a is the modulation frequency, equal to 2π times the bit rate. Eqn (17) can be written in the form (12), with the perturbation $P(\psi, \psi^*)$ given by the expression

$$P(\psi, \psi^*) = (1 - \varkappa_3)\psi + \varkappa_1\psi_{tt} + \varkappa_3\cos(\Omega_a t)\psi, \quad (18)$$

where $\varepsilon = i\delta$; $\varkappa_3 = \mu_a/\delta$.

Before dealing with a more complex case of two-soliton propagation, let us gain some qualitative insight into this problem by considering the one-soliton propagation through the system comprising both BLA and AM. To do this, let us apply the adiabatic perturbation method to

$$\psi_0(z, t) = \eta\,\mathrm{sech}\eta[t - \rho(z)]\exp\{i[\zeta t + \varphi(z)]\}, \quad (19)$$

where $\rho(z) = 2\xi z + \rho_0$; $\varphi(z) = (\eta^2 - \xi^2)z + \varphi_0$; $\rho_0 = \ln(|\gamma_0|)/\eta$; and $\varphi_0 = \arg(\gamma_0)$. Then the dynamics of the soliton parameters is governed by the set of equations [17]:

$$\frac{d\eta}{dz} = 4(\delta - \mu_a)\eta - 4\beta\eta\left(\frac{\eta^2}{3} + \zeta^2\right)$$

$$+ 2\pi\Omega_a\mu_a\cos(\Omega_a\rho)\mathrm{cosech}\left(\frac{\pi\Omega_a}{2\eta}\right), \quad (20)$$

$$\frac{d\zeta}{dz} = -\frac{8}{3}\beta\eta^2\zeta, \quad (21)$$

$$\frac{d\rho}{dz} = 2\zeta + \frac{2\pi\mu_a}{\eta}\sin(\Omega_a\rho)\mathrm{cosech}\left(\frac{\pi\Omega_a}{2\eta}\right)$$

$$\times\left[1 - \frac{\pi\Omega_a}{2\eta}\coth\frac{\pi\Omega_a}{2\eta}\right]. \quad (22)$$

Obviously, this system has a fixed point at $(\eta, \xi, \rho) = (\eta_0, 0, 0)$ if

$$\delta - \mu_a - \frac{\beta\eta_0^2}{3} + \frac{\pi\Omega_a}{2\eta_0}\mu_a\mathrm{cosech}\left(\frac{\pi\Omega_a}{2\eta_0}\right) = 0, \quad (23)$$

and the fixed point is stable if

$$\frac{3\pi\Omega_a}{4\eta_0^3}\mu_a\mathrm{cosech}\left(\frac{\pi\Omega_a}{2\eta_0}\right)\left[\frac{\pi\Omega_a}{2\eta_0}\coth\frac{\pi\Omega_a}{2\eta_0} - 1\right] < \beta. \quad (24)$$

Since the two-soliton state breaks after a short distance in two solitons, which can be viewed as being rather independent, Eqns (20)–(22) are expected to give a fairly good qualitative description of the asymptotic behavior of the two emerging solitons. Therefore, when we chose the parameters δ, β, μ_a, and Ω_a for the numerical simulations of Eqn (17), we have been guided by Eqn (23). However, it is necessary to bear in mind that in the case of two-soliton solutions, the asymptotic time shift ρ is no longer zero, so that the asymptotic state of the emerging solitons cannot be the fixed point $(\eta_0, 0, 0)$. Moreover, Eqn (23) does not take into account the mutual interaction between the asymptotic solitons, so that we cannot expect that it is rigorously verified by the asymptotic values of the parameters of the emerging solitons.

For a more detailed analysis of the propagation of the two-soliton solutions (3) and (8) in the presence of the BLA and the amplitude modulation, Eqn (17) is integrated numerically for a set of parameters δ, β, μ_a, and Ω_a. The numerical integration shows that for both cases (symmetric and antisymmetric), the asymptotic value of the amplitude η of the emerging solitons increases as the modulation frequency Ω_a decreases, which agrees with Eqn (23). Moreover, we observed that as the modulation amplitude μ_a increases, the soliton propagation becomes more unstable, in agreement with Eqn (24).

Fig. 6 represent the results obtained by using the adiabatic perturbation method for the symmetric (antisymmetric) case. One can see that though the adiabatic perturbation method gives a good qualitative description of the soliton propagation, unlike the previous case, the quantitative results obtained by the two methods do not agree so well. This can be explained by the emission of a larger amount of radiation.

4. Superposition of N solitons

Since in the optical networks, which are presently in use, the optical signal is transmitted over several frequency channels, it is natural to ask how the results presented in the preceding sections can be extended to the case of soliton propagation in N different channels. In order to address

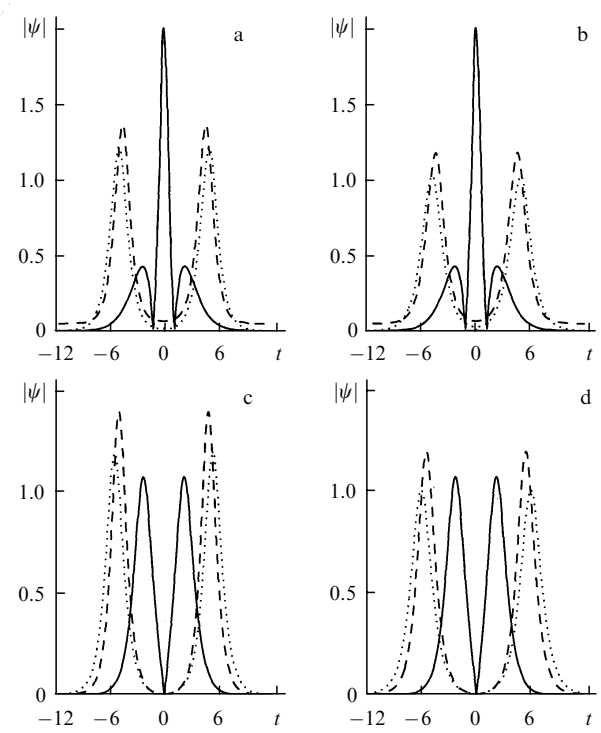

Figure 6. The amplitude $|\psi|$ of the symmetric soliton (3) with $\eta(0) = 1$, $\xi(0) = 0.2$, $\rho_0(0) = 0$, $\phi_0(0) = \pi/2$ [(a) and (b)] and of the antisymmetric soliton (8) with $\eta(0) = 1$, $\xi(0) = 0.2$, $\rho_0(0) = \phi_0(0) = 0$ [(c) and (d)]: input pulse (solid curve), numerical simulations (dashed curve), adiabatic perturbation method (dotted curve); $\beta = 0.06$ and $\mu_a = 0.01$ (a) $\delta = 0.039$, $\Omega_a = 2\pi/20$; (b) $\delta = 0.038$, $\Omega_a = 2\pi/10$; (c) $\delta = 0.039$, $\Omega_a = 2\pi/20$; (d) $\delta = 0.038$, $\Omega_a = 2\pi/10$.

this problem, let us consider the superposition of N single solitons with different frequencies,

$$\psi(0, t) = \sum_{k=1} \operatorname{sech} t \exp\{\mathrm{i}[k - (N+1)/2] \times [\omega t + \theta/(N-1)]\}, \tag{25}$$

where N is the number of solitons, ω is the frequency detuning between adjacent solitons, and θ is the total phase shift between the first and the last soliton.

The first fact observed when the number of solitons N is increased is that the structure of the soliton spectra of the emerging field becomes highly intricate. In order to illustrate this, we present in Fig. 7 the soliton spectra which correspond to $N = 4$ and $N = 8$, respectively. We mention that all these spectra correspond to the input pulses (25) for which the phase shift $\theta = 0$. As a check of these numerical results, we verified that for each value of the frequency detuning the equality $E_{in} = E_{rad} + E_{sol}$ is satisfied. As another test of the validity of the spectra in Fig. 7, we used the initial condition (25) for various values of the parameters N and ω and, for all values, we obtained an optical field with the structure implied by Fig. 7.

As a general remark related to Fig. 7, we mention that, as in the case $N = 2$, in order to obtain N solitons with distinct frequencies (as necessary in a WDM scheme) the frequency detuning ω must be larger than a certain threshold value. Furthermore, our numerical simulations show that, as the number N of channels increases, the threshold frequency detuning increases. For example, for $N = 2$ the critical frequency detuning is $\omega_{cr} = 3.018$, for $N = 4$ the

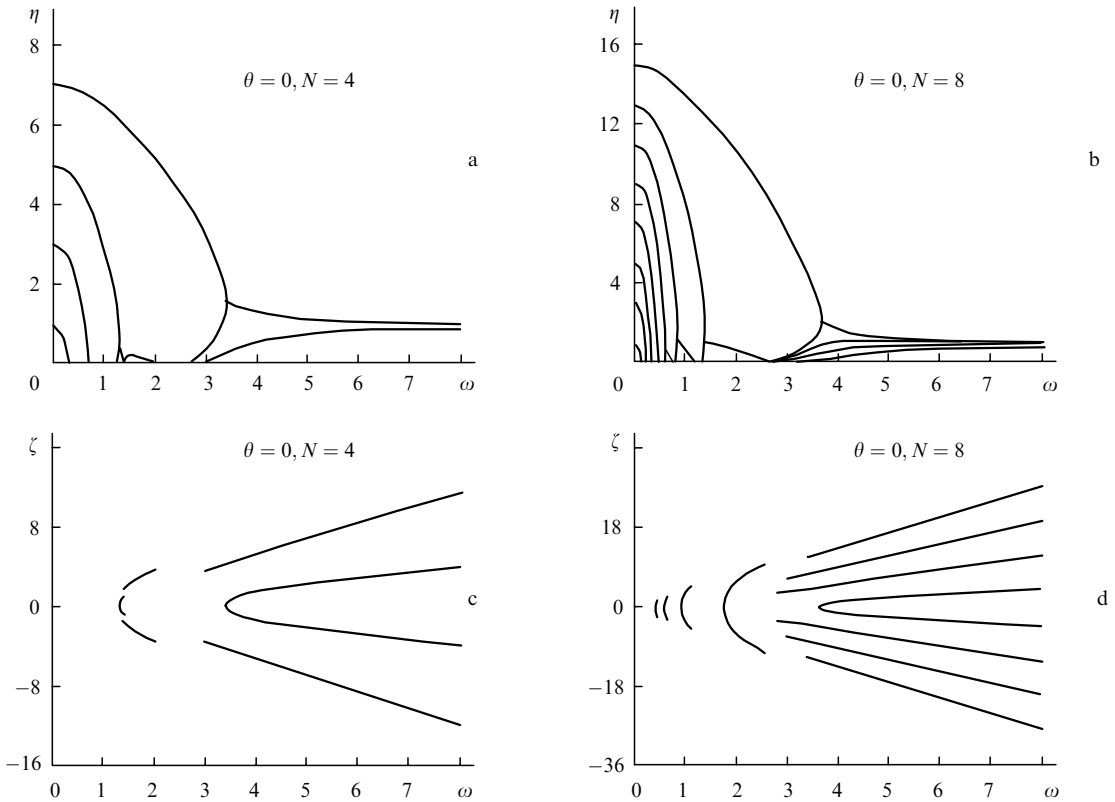

Figure 7. The soliton spectrum determined by the input (25) with $\theta = 0$ vs frequency detuning: (a) The soliton amplitude for $N = 4$ solitons, and (b) for $N = 4$ solitons. The soliton velocity vs detuning (c) for $N = 8$ solitons, and (d) for $N = 8$ solitons.

critical frequency detuning is $\omega_{cr} = 3.385$, while for $N = 8$ it is $\omega_{cr} = 3.629$.

In what follows, we discuss the changes which are introduced in the soliton spectra by the initial time shift between the solitons in different channels [optical time-division multiplexing (OTDM)]. Consider the superposition of the two solitons:

$$\psi(0, t) = \operatorname{sech}(t - T_0) \exp(i\omega t/2), \tag{26}$$

where $2T_0$ is the time separation between the solitons. For simplicity, we assume that both solitons have the same input phase ($\theta = 0$).

The soliton spectra corresponding to $T_0 = 0$ and $T_0 = 1$ are presented in Figs 8a and 8b, respectively. As the time shift increases from 0 to 1, the overlap between solitons decreases, the soliton interaction becomes weaker, and, in turn, the critical frequency shift is seen to decrease from $\omega_{cr} = 3.018$ to $\omega_{cr} = 1.72$. As an important consequence of this decrease in the interchannel frequency separation is the increase in the transmission capacity of the WDM system. On the other hand, by introducing the time shift T_0, the temporal bit window widens and, consequently, the transmission capacity tends to decrease. However, it is not difficult to see that the combined action of these two competing factors is a net increase in the transmission capacity of the WDM system. Consider an optical fibre for which the soliton repetition period is $\Delta t = m\tau$ (in practical applications $m \leqslant 10$) and the interchannel frequency separation is ω. The transmission capacity per channel is inversely proportional to the repetition period Δt, and the total transmission capacity of the line is proportional to the number of channels N, or, in other words, inversely proportional to the frequency interchannel separation ω. Therefore, the total transmission capacity R is inversely proportional to the product $\omega\Delta t$. Furthermore, suppose that ω is chosen to be equal to the critical frequency $\omega_{cr} = 3.018$, which corresponds to $T_0 = 0$. We emphasise here that although ω_{cr} is not the lowest frequency separation that can be used in a reliable WDM system (a larger frequency separation ω would be needed for the effect of initial overlap to be rendered insignificant), it represents a very useful parameter for estimating the upper bound of the bit rate R. Now, if we introduce the time shift T_0 and require that the time separation between adjacent solitons remains the same (equal to $m\tau$), the repetition period becomes $\Delta t' = m\tau + 2T_0$ and the frequency separation $\omega = \omega'_{cr} = 1.72$. Thus, the ratio of the bit rates is

$$\frac{R'}{R} = \frac{m\tau\omega_{cr}}{(m\tau + 2T_0)\omega'_{cr}}. \tag{27}$$

Therefore, for $m = 10$ a combination of OTDM and WDM gives an increase in the bit rate of about 50 %. As the last comment related to this problem, we mention that we expect that the above conclusion remains valid for $m \geqslant 10$ and for time shifts T_0 not too large. This is so because if the parameters m and T_0 are in this range, the improvement in the bit rate due to the reduction of ω_{cr} overcomes the bit rate reduction due to the increase in the bit window. However, as the determination of the soliton spectra is very time consuming, we restricted our numerical investigations to the example presented above.

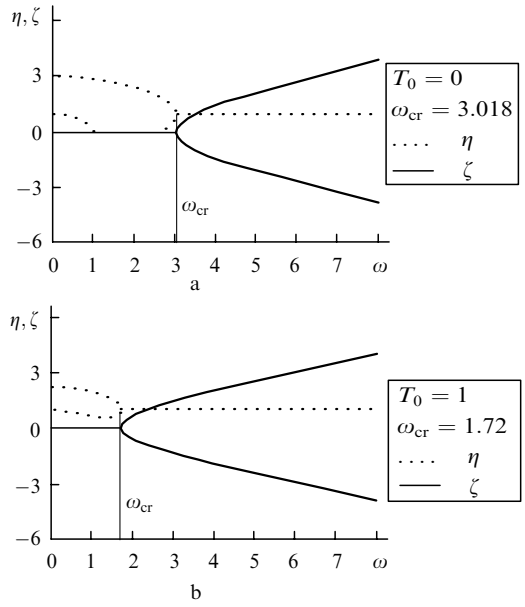

Figure 8. The soliton spectrum determined by the input (26).

5. Conclusions

We have demonstrated that, by using the adiabatic perturbative method, many of the properties of multiwavelength optical pulse propagation through various communication systems can be explained more thoroughly than in previous studies. The most important result is that we are able to relate an emerging field structure to an input superposition of a rather general form. This relation provides a more clear interpretation of the interaction of optical solitons endowed with symmetry. Using our analytical solutions, we are able not only to explain some of our results obtained by numerical simulations, but also to obtain a quantitative understanding of the physical processes which take place in a multi-channel WDM optical transmission system.

Note that the problem of the dynamics of a two-wavelength pair of optical solitons appears in a number of other applications, not just in WDM communication lines; for instance, in the case of passively mode-locked solid-state lasers, when different-color pulses are generated from a single gain medium. Thus, recently it has been shown that the retarded coherent response of such an amplifier may essentially change the behavior of two-frequency solitons from that predicted by a standard soliton perturbation theory [18]. Devices like these may find applications as sources for generation of THz trains of narrow-band optical pulses.

Acknowledgements. We highly appreciate valuable contribution made to this work by L.-C. Crasovan, F. Ginovart, and D. Mazilu. Useful discussions with M.J. Ablowitz, S. Blair, G. Biondini, V.M. Eleonsky, R.M. Osgood, Jr., and V.A. Vysloukh are gratefully acknowledged, too. This work was supported in part by the CIES program, France, CONACyT, Mexico, DFG, Germany, and the Russian Foundation for Basic Research.

References

1. Mollenauer L.F., Mamyshev P.V., Neubelt M.J. *Proc. Conf. Opt. Fiber Commun. (OFC'96)* (San Jose, Cal., USA, February 1996, Paper PD22).
2. Nakazawa M., Suzuki K., Kubota H., Sahara A., Yamada E. *Electron. Lett.*, **33**, 1233 (1997).
3. Idem. *Electron. Lett.*, **27**, 695 (1991).
4. Kodama Y., Hasegawa A. *Opt. Lett.*, **16**, 208 (1991).
5. Friberg S. *Opt. Lett.*, **16**, 1484 (1991).
6. Mamyshev P.V., Mollenauer L.F. *Opt. Lett.*, **21**, 396 (1996).
7. Andrekson P.A., Olsson N.A., Simpson J.R., Tanbun-Ek T., Logan R.A., Becker P.C., Wecht K.W. *Appl. Phys. Lett.*, **57**, 1715 (1990).
8. Andrekson P.A., Olsson N.A., Simpson J.R., Tanbun-Ek T., Logan R.A., Wecht K.W. *J. Lightwave Technol.*, **9**, 1132 (1990).
9. Olsson N.A., Andrekson P.A., Simpson J.R., Tanbun-Ek T., Logan R.A., Wecht K.W. *Electron. Lett.*, **26**, 1499 (1990).
10. Mollenauer L.F., Evangelidis S.G., Gordon J.P. *J. Lightwave Technol.*, **9**, 362 (1991).
11. Panoiu N.-C., Mihalache D., Mazilu D., Crasovan L.C., Mel'nikov I.V., Lederer F. *Chaos*, **10**, 625 (2000).
12. Boffetta G., Osborne A.R. *J. Comput. Phys.*, **102**, 252 (1992).
13. Panoiu N.-C., Mel'nikov I.V., Mihalache D., Etrich C., Lederer F. *Phys. Rev. E*, **60**, 4868 (1999).
14. Kodama Y., Romagnoli M., Wabnitz S. *Electron. Lett.*, **28**, 1981 (1990).
15. Matsumoto M., Ikeda H., Uda T., Hasegawa A. *J. Lightwave Technol.*, **13**, 658 (1995).
16. Nakazawa M., Yamada E., Kubota H., Suzuki K. *Electron. Lett.*, **27**, 1270 (1991).
17. Hasegawa A., Kodama Y. *Solitons in Optical Communications* (Oxford: Oxford University Press, 1995).
18. Mel'nikov I.V., Mihalache D., Panoiu N.-C., Ginovart F., Zamudio Lara A. *Opt. Commun.*, **191**, 133 (2001).